Strain Measurements of Chondrules and Refractory Inclusions in Allende

#1309

Alastair W. Tait[1], Kent R. Fisher[2], Justin I. Simon[3]

[1]Monash University, Clayton, 3168, Vic., Australia. [2]University of Cincinnati, Cincinnati, OH, 45219, USA. [3]Center for Isotope Cosmochemistry and Geochronology, ARES, NASA Johnson Space Center, Houston, TX, 77058, USA.

Introduction

This study uses traditional 2D strain measurement techniques laid out by Cain et al. (1986), as well as new 3D techniques leveraging X-ray Computed Tomography (CT), to evaluate petrographic textures in the Allende CV3 chondrite for preferred orientation, and to quantify the strain in Allende.

The existence of petrofabrics and lineations was first observed in carbonaceous meteorites in the 1960's (Dodd, 1965). Yet, fifty years later only a few studies have reported that meteorites record such features (e.g., Sneyd et al., 1988). Impacts are often cited as the mechanism for this feature (Stoffler et al., 1991), although plastic deformation from overburden and nebular imbrication have also been proposed (Dodd, 1965; Sneyd et al., 1985; Cain et al., 1986).

Methodology

The 2D and 3D strain analysis techniques employed by this research looked at the major phases (CAIs, Chondrules, Chondrule Rims and Matrix) to understand the amount of deformation that has occurred. To do this a ~27 cm slab of Allende was photographed at 13.88 µm/px on both sides, with the CAIs digitized in Adobe Illustrator (Srinivasan et al., 2013). Additional phases from a statistically relevant medium selection, were digitised multiple times by different workers with the sample image oriented at different angles to eliminate collection biases. These data were exported into ImageJ, an image analysis software program (Rasband, 1997), and underwent particle analysis to extract physical characteristics of grains: Coordinates, area, major axis, minor axis, angle, circularity and solidity. For the 3D analysis techniques, the slab was also subjected to X-ray Computed Tomography at NASA JSC with a resolution of 173.91 µm/voxel.

2D Strain Analysis

On all phases except the matrix, the ratio between the major and minor axial lengths was used to establish shortening. Harmonic means were used to reduce the effect of outliers biasing the results. Different phases recorded different amounts of shortening (Table 1) and all phases record deformation in the same NE-SW orientation as determined by plotting the long axis of phases into a rose diagram (Fig. 1). The strain partitioning was Chondrule>Matrix>Rims>CAIs. Evidence of this can be seen in Figure 2C, with a CAI wrapping around a more competent chondrule.

To evaluate the whole rock (matrix) deformation, Fry diagrams were used (Fig. 2A) (Fry, 1979). Chondrules were measured because of their competency and assumed initial circularity (Martin and Mills, 1976; Sneyd et al., 1985). A strike of 38° consistent with the orientation of the particle-defined petrofabric and a uniaxial shortening of 20% was recorded by the matrix.

Previous work has show that in the Fine Grained Rims (FGR) of chondrules there is a distinct LPO (Lattice-Preferred Orientation) alignment of olivine grains creating an augen texture (Bland et al. 2011). We observed via SEM element maps that Ca-rich pyroxenes in the matrix, away from the FGR are deforming around grains as well, which would indicate a whole rock deformation (Fig. 2B)

Rims of the chondrules were measured and found to be more deformed than the matrix and the chondrules themselves (20% and 24%, respectively vs. 17%) (Table 1). This indicates that the formation of the rims predate the deformation and supports the argument that these formed in the nebula (Bland et al. 2011).

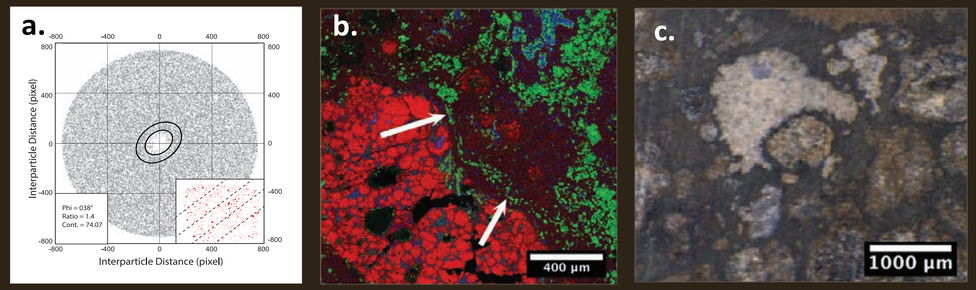

Fig 2. (a) Fry diagram shows the degree of deformation of the matrix. The central ellipse records a strike of 38° and an axial ratio of 1.4. Inset: Represents the strike, overprinted on the slab of Allende with CAIs in red. (b) SEM element map image. Ca (Green), Al (Blue), Mg (red) with 'augen' alignment of Ca-rich pyroxenes. Arrows point out deformation and long axis elongation of pyroxene. Pyroxenes are secondary and therefore may have formed during or after deformation. (c) Shows a photograph of a CAI wrapping around a more competent chondrule, indicating different phase competencies

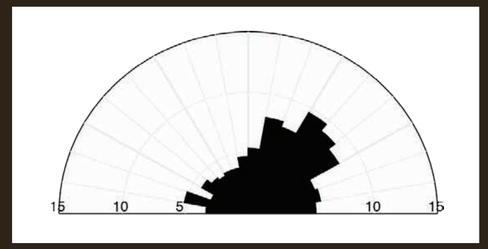

Fig 1. This rose diagram plots the angle of the Major axis of CAIs (relative to the top of the image = 0°) on a half circle of 180 in buckets of 10°. CAIs recorded a maximum value between 30-40° which is within the range of the Fry Plot results for chondrules (Fig 1a) and the CAI lineation's vector (Fig 4b).

Table 1 - Phase Strain Values

Phase	(Observer 1) (Axial Ratio)	(Observer 2) (Axial Ratio)	σ	±SE	Minimum Mean (Axial Ratio)	Uniaxial Shortening (%)
Chondrule	1.32	1.33	0.31	0.01	1.33	16.6
CAI	1.70	1.66	0.64	0.03	1.68	29.2
Rim	1.50	1.50	0.75	0.09	1.50	23.7
Matrix	–	–	–	–	1.40	20.1

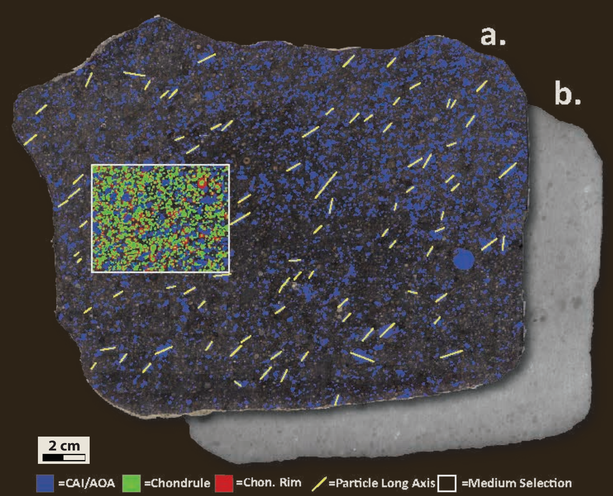

Fig 3. (a) This 27 cm wide slab of Allende, was photographed and stitched together at 13.88 um/px. CAIs (blue) were previous digitised across the whole slab (Srinivasan et al.,2013). Yellow lines have been drawn over the long axis of selected CAIs to help the viewer visualise the strike of the petrofabric. (b) This image represents a stacked series (n=30) of X-ray Computed Tomography (CT) images. (c) A statistical representative region was selected for further digitisation of Chondrules (green), their Rims (Red) and CAIs (blue).

3D Strain Analysis

3D strain analysis was made possible by X-ray Computed Tomography (CT) at NASA JSC. A series of completely encapsulated CAIs (n=19) were digitised and imported into imageJ where we used BoneJ (Doube et al., 2010), a plugin for imageJ, that objectively fits an ellipsoid to a 3D mesh (Fig. 4A). Directional cosines that were extracted form the long-axis of the encapsulated CAIs were then plotted on a steronet plot showing a mean lineation trend of 214.07° and a plunge of 3.44° (Fig. 4B). The back angle of the lineation is 34°, which is consistent with the whole rock.

The initial axial ratio(s) of CAIs is unknown, which means it is near impossible to establish an absolute amount of shortening. However it is possible to establish a maximum amount of shortening if one assumes an initial axial ratio of 1:1:1. Flinn's method was employed to measures the strain of the particles in 3D by plotting the strain axis of an ellipsoid X/Y and Y/Z (Flinn, 1962).

The results showed axial ratios of X/Y = 1.42, Y/Z = 3.69, and X/Z = 5.26. This translates to a uniaxial shortening of 49%. The shape descriptor k is used to describe the shape of the strain ellipsoid, the value k = 0.27 puts it in the oblate field (Fig. 4C). The average dip of the CAIs was: 17.56° ± 4.81° to the west, relative to the surface of the Allende slab.

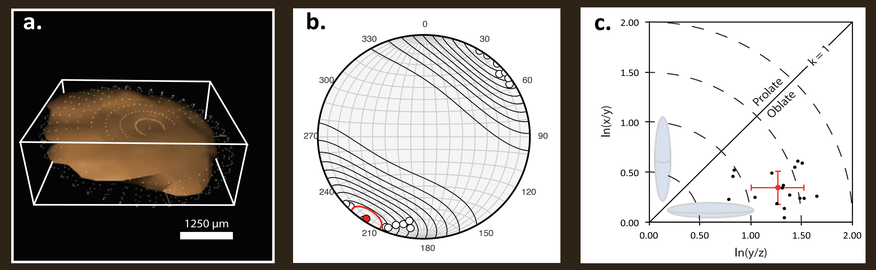

Fig 4. (a) This image shows one (n=17) reconstructed mesh of a fully encapsulated CAI particle. The particle was reconstructed by CT generated cross sections. An ellipsoid was objectively fit to the particle with boneJ. The characteristics of the CAI were then exported to Excel for further analysis. **(b)** This stereonet shows a strong lineation from the North-East to the South-West. The red data point is the mean vector, surrounded by a Brigham 99% confidence cone (red). Additional Kamb contours exist out to 3σ. **(c)** This Flynn diagram shows that CAIs in Allende plot strongly in the oblate (flattening field) with the shape descripter term k = 0.27. The red value is the arithmetic mean, with standard deviation out to 2σ. Plotting in the oblate field is a strong indicator of simple shear.

Discussion

Multiple strain techniques across multiple phases are in agreement of a NE-SW fabric in Allende (relative to the top of the slab). The whole rock Fry diagram and the CAI Rose diagrams give a strike of 038° and 031-040°, respectively. Additionally, the encapsulated CAIs give a trend of 214°, with a back angle of 034°. It is hard to fathom of a nebular process that could create common lineations and uniaxial deformations in all phases of the meteorite. However, it is quite reasonable to assume high aspect ratio particles from previous nebular deformation events (e.g., Lorenz et al. 2012) would be exacerbated by parent body deformation events such as distal impacts, crater-wall slumping or overburden, once they accreted on the surface of the parent body.

Conclusions

- Allende has undergone pure-shear shortening of ~ 20%. Phases inside Allende partition strain differently with chondrules exhibiting the least (~16.6% uniaxial shortening) and CAIs the most (≤49% uniaxial shortening) apparent deformation.
- Agreement exists between multiple 2D and 3D strain techniques of a NE to SW fabric relative to the top of the Allende slab, which suggests a common deformation process that likely happened on the parent body. However, flattening observed in Allende CAIs may have initiated in the nebula (cf. Ivanova et al. this meeting).

Contact

Alastair Tait
Monash University
alastair.tait@monash.edu

Acknowledgment

This work supported by a NASA Cosmochemistry grant to PI JIS, the Astromaterials and Space Exploration Research Office at the Johnson Space Center, the Lunar Planetary Institute for Tait's Summer 2013 internship and the NASA Co-op program that supports Fisher's internship. Joesph Minafra generously loaned the Allende slab from his personal collection used in this research.

References

1. BLAND, P.A., HOWARD, L.E., PRIOR, D.J., WHEELER, J., HOUGH, R.M., AND DYL, K.A. 2011. Earliest rock fabric formed in the Solar System preserved in a chondrule rim. *Nature Geoscience*, 4, 244–247.
2. CAIN, P.M., MCSWEEN, H.Y., JR, AND WOODWARD, N.B. 1986. Structural deformation of the Leoville chondrite. *Earth and Planetary Science Letters*. **77**, 165–175.
3. DODD, R.T., JR. 1965. Preferred orientation of chondrules in chondrites. *Icarus*. **4**, 308–316.
4. DOUBE, M., KLOSOWSKI, M.M., ARGANDA-CARRERAS, I., CORDELIERES, F., DOUGHERTY, R.P., JACKSON, J., SCHMID, B., HUTCHINSON, J.R., AND SHEFEBINE, S.J. 2010. BoneJ: free and extensible bone image analysis in ImageJ. *Bone*. **47**, 1076–1079.
5. FLINN, D. 1962. On Folding During Three-Dimensional Progressive Deformation, *Quarterly Journal of the Geological Society*. **118**, 385–428.
6. FRY, N. 1979. Random point distributions and strain measurement in rocks. *Tectonophysics*. **60**, 89-105.
7. IVANOVA, M.A., LORENZ, C.A., SHUVALOV, V.V., KROT, A.N., MACPHERSON, G.J., AND BIZZARRO, M. 2014. Plastically-Deformed Igneous Calcium-Aluminum-Rich Inclusions From CV Carbonaceous Chondrites: Clues to a Nature of CAI Melting Events. *LPSC XLV*. 2166
8. LORENZ, C.A., IVANOVA, M.A.,SHUVALOV, V.V., 2012. Aerodynamic Deformation of Molten CAIs as a Possible Mechanism of Early Solids Processing in The Solar Nebula. *75th Annual Meteorittical Society Meeting*. *5027*
9. MARTIN, P.M., AND MILLS, A.A. 1976. Size and shape of chondrules in the Bjurböle and Chainpur meteorites. *Earth and Planetary Science Letters*. **33**, 239–248.
10. RASBAND, W.S. 1997. ImageJ. *U.S. National Institute of Health*.
11. SNEYD, D.S., MCSWEEN, H.Y., JR, AND LABOTKA, T.C. 1985. Strain Analysis of the Parnallee unequilibrated ordinary chondrite. *LPSC XVI*, pp. 797–798.
12. SNEYD, D.S., MCSWEEN, H.Y., JR, SUGIURA, N., STRANGWAY, D.W., AND NORD, G.L., JR. 1988. Origin of Petrofabrics and Magnetic Anisotrop in Ordinary Chondrites. *Meteoritics*. **23**, 139–149.
13. SRINIVASAN, P., SIMON, J.I., AND CUZZI, J.N. 2013. Refractory Inclusion Size Distribution and Fabric Measured in a Large Slab of the Allende CV3 Chondrite, *LPSC XLIV*, 2580
14. STOFFLER, D., KEIL, K., AND EDWARD, R. 1991. Shock metamorphism of ordinary chondrites. *Geochimica et Cosmochimica Acta*. **55**, 3845–3867.